



**HAL**  
open science

# Numerical modeling of unsteady partial cavities behind a backward facing step

Thierry Maître, Christian Pellone

► **To cite this version:**

Thierry Maître, Christian Pellone. Numerical modeling of unsteady partial cavities behind a backward facing step. CAV 2001: Fourth International Symposium on Cavitation, Jun 2001, Pasadena, United States. hal-00266177

**HAL Id: hal-00266177**

**<https://hal.science/hal-00266177>**

Submitted on 14 Jan 2020

**HAL** is a multi-disciplinary open access archive for the deposit and dissemination of scientific research documents, whether they are published or not. The documents may come from teaching and research institutions in France or abroad, or from public or private research centers.

L'archive ouverte pluridisciplinaire **HAL**, est destinée au dépôt et à la diffusion de documents scientifiques de niveau recherche, publiés ou non, émanant des établissements d'enseignement et de recherche français ou étrangers, des laboratoires publics ou privés.

# NUMERICAL MODELLING OF UNSTEADY PARTIAL CAVITIES BEHIND A BACKWARD FACING STEP

THIERRY MAÎTRE, CHRISTIAN PELLONE

LABORATOIRE DES ECOULEMENTS GÉOPHYSIQUES ET INDUSTRIELS, BP 53, 38041 GRENOBLE CEDEX 9, FRANCE

TÉL: +33 (0)4 76 82 50 39

FAX: +33 (0)4 76 82 52 71

EMAIL: PELLONE@HMG.INPG.FR

## ABSTRACT

This paper presents some calculation results in the cases of steady and non-steady partial cavity. These results are obtained with the commercial Navier-Stokes codes FLUENT and STAR-CD and compared with experimental results. Under cavitation conditions the first code uses a bubbles two-phase model. The second code uses the VOF (volume of fluid) technique to calculate the interface and allows the use of either the barotropic or the bubbles two-phase model. Different arrangements of the three parameters step height, channel confinement and cavitation number are examined. Cavities observed experimentally are compared with that obtained by the calculation. We investigate the ability of the models to reproduce the non-steady behaviours (re-entrant jet thickness, shedding frequencies).

## Nomenclature

a	Speed of sound in water	(m/s)	Se	Area of the confinement section (Se)	(m <sup>2</sup> )
a <sub>v</sub>	Speed of sound in vapour	(m/s)	Se'	Area of the upper section (Se')	(m <sup>2</sup> )
C <sub>p</sub>	Pressure coefficient	()	V <sub>e</sub>	Velocity in the confinement section	(m/s)
D <sub>0</sub>	Tunnel width	(mm)	V <sub>0</sub>	Velocity in the inlet section (Si)	(m/s)
e	Confinement height	(mm)	V <sub>r</sub>	Reference velocity	(m/s)
h	Step height	(mm)	V	Velocity vector	()
H <sub>0</sub>	Tunnel height	(mm)	β	Divergent angle	(deg)
L	Cavity length	(mm)	μ	Molecular viscosity of water	(kg/(m.s))
N	Bubble number density per unit volume	(m <sup>-3</sup> )	μ <sub>v</sub>	Molecular viscosity of vapour	(m <sup>2</sup> /s)
P	Pressure	(Pa)	ρ	Density of the water	(kg/m <sup>3</sup> )
P <sub>r</sub>	Reference pressure	(Pa)	ρ <sub>v</sub>	Density of the vapour	(kg/m <sup>3</sup> )
P <sub>v</sub>	Vapour pressure	(Pa)	σ	Cavitation number	()
P <sub>0</sub>	Pressure in the inlet section (Si)	(Pa)	∇	Divergence operator	()
Si	Area of the inlet (Si) & outlet (So) sections	(m <sup>2</sup> )			

## 1. INTRODUCTION

Attached cavities are more or less unsteady and unstable. In particular, cavitation instabilities often occur in a turbomachinery and induce abnormal dynamic behaviours, noise and erosion. Among several kinds of instabilities that may occur in cavity flows, one of the most important is the development of a re-entrant jet at the end of the cavity (Knapp *et al.*, 1970, Furness & Hutton, 1975). Knapp *et al.* (1970) give a precise description of the flow at the downstream end of a cavity. In this region the liquid hits the wall and locally divides into two parts. The adverse one gives birth to the re-entrant jet, whereas the other one, in the direction of the main flow, makes the liquid flow re-attach to the wall. Furness & Hutton (1975) describe and modelize the dynamic behaviour of the cavity which develops on a Venturi-type nozzle by a two-dimensional unsteady potential flow theory. The theory holds true for the early formation of the re-entrant jet, but is unable to model the shedding of a cloud when the re-entrant jet intersects the cavity interface.

The flow structure analysis around unsteady cloud cavitation shows that the shedded cloud is a large-scale vortex structure containing many small cavitation bubbles (Kubota *et al.*, 1989, Yamaguchi *et al.*, 1990). The generation mechanism of cloud cavitation was studied in detail by Kawanami *et al.* (1997). This study definitely confirms the essential role of the re-entrant jet on the onset of cloud cavitation. The study (Reboud *et al.*, 1998) highlights the

structure of the two-phase flow inside the cavity using a double optical probe. The local void fraction and the velocity measurements confirm the existence of a reversed two-phase flow along the wall.

From a modelling viewpoint, the main difficulty relates to the strong coupling between the pressure field and the vapour fraction. In addition, an accurate model should take into account both the compressible behaviour of the two-phase medium and the non-compressible behaviour of the pure liquid. It should also be able to describe the growth phase of the sheet cavity, the development of the re-entrant jet, the break-off and the fully detached cloud. Under unsteady configurations several approaches were used to model the two-phase fluid as an homogeneous fluid of variable density. Kubota *et al.* (1992) describe the evolution of the bubble cluster and computes the void fraction. Reboud & Delannoy (1994) use an arbitrary barotropic equation of state to describe the behaviour of the mixture. Diéval *et al.* (1998) develop a separated two-phase flow model using a free surface tracking method (volume of fluid, named VOF) to capture the interfaces.

In this paper we present recent numerical results obtained by the commercial codes FLUENT and STAR-CD and compared with the experimental results obtained by Callenaere *et al.* (1998). In this last study the authors highlight the different patterns of partial cavities, yield the re-entrant jet thickness and pressure fluctuation measurements just as the cavity evolution in the periodic case. In this study, it appears of primary importance to know the adverse pressure gradient at cavity closure.

In the framework of the FLUENT code, a two-phases homogeneous flow model is used. In this model the inside and the outside of the cavity is treated as a mixture. In this approach, the momentum and continuity equations for the mixture are solved. A simplified Rayleigh equation applied to a cluster of identical bubbles is used to evaluate a mass transfer term between the two phases. The model does not assume that there is an interface between two immiscible fluids; it allows the fluids to be interpenetrating. The volume fractions of the two phases, for a control volume, can therefore be equal to any value between 0 and 1, depending on the space occupied by the two phases.

In the framework of the STAR-CD code the VOF model is used. It is a fixed grid technique for two fluids where the position of the interface is of interest. The formulation relies on the fact that the two phases are not interpenetrating (Hirt & Nichols, 1981). A variable is introduced, the volume fraction of one of the phases in the computational cell. The position of the liquid-vapour interface is determined by solving the volume fraction transport equation in which a source term is introduced. This term is representative of the vapour production rate, depends on the local pressure and is determined by the cavitation model. The barotropic and the two-phase models are used. For the barotropic model an analytical relation between the pressure and the void fraction is used (Schmidt *et al.*, 1997). For the bubble two-phase model a Rayleigh-Plesset equation is applied to a cluster of bubbles (Kubota *et al.*, 1992).

All the calculations are performed under turbulent conditions using the standard  $k-\epsilon$  model and wall functions. The results are analysed in order to verify the ability of the calculation to reproduce the main features of the cavitating flow. Particularly, the thickness and the velocity of the re-entrant jet and the Strouhal number are compared to experimental values.

## 2. EXPERIMENTAL TUNNEL CONFIGURATION

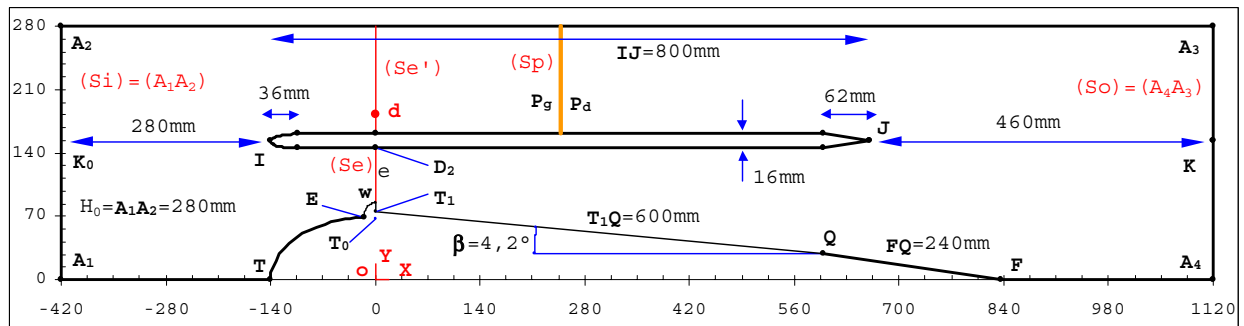
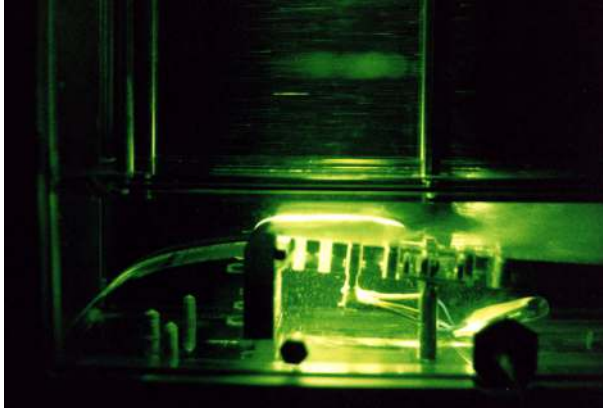


Figure 1. Schematic view of the test tunnel.

The experimental study was conducted in the hydrodynamic tunnel of the Laboratoire des Écoulements Géophysiques & Industriels of Grenoble (Briçon-Marjollet & Michel, 1987). For the present study, the test section, used in closed mode, is  $H_0 = A_1A_2 = 280$  mm high and  $D_0 = 175$  mm wide (figure 1). The tunnel bottom consists of a quarter-ellipse-shaped nose topped by a tiny quarter-circle-shaped obstacle. The ellipse sides values are respectively  $OT = 140$  mm and  $OT_0 = 70$  mm. The quarter-circle radius value is  $T_0w = T_0E = 15$  mm, where point E is the intersection point between the quarter-circle and the quarter-ellipse. The tiny obstacle creates a stagnation

point directly upstream of the cavity and consequently generates a laminar flow close to the beginning of the cavity. Located downstream of the nose, a flat plate (T<sub>1</sub>Q), 600 mm long, can be moved vertically ( $h = T_1w$ ) and positioned at incidence  $\beta$ . The plate (T<sub>1</sub>Q) is joined with a smaller one (QF), 240 mm long, intersecting the tunnel bottom at point F. This arrangement leads to a diverging step of adjustable height  $h$ . An additional horizontal plate (IJ), 800 mm long and 16 mm thick, is set above the step to change the confinement height  $e = wD_2$ . The leading edge I and the nose T of the quarter-ellipse are in the same cross-section. This confinement plate is tooled in its rear part by a chamfered-edge 62 mm wide and in its front part by a half-ellipse 36 mm main radius. It is fixed in place by 8 rods, 12 mm in diameter and originating from the tunnel ceiling. The figure 2 shows a photographic insight focused on the cavity region.



**Figure2. Photo of the region of interest.**

Notice that, these rods in the upper channel generate substantial head losses. In effect, the lower channel flow rate is not the same as that the one obtained without rods. Consequently, a numerical calculation has to insure the correct experimental flow rate in the lower channel. Three geometrical parameters are controlled in the present configuration:

- the step height  $h$ , varying from 0 to 12 mm, which controls the cavity thickness;
- the slope  $\beta$ , varying from 0 to 4.2°, which controls the divergence and so the adverse pressure gradient;
- the confinement height  $e$ , varying from 20 to 60 mm, which is an additional way to change the pressure distribution.

In comparison with classical venturis (Furness & Hutton, 1975), the present configuration allows to get various cavity patterns, including self-pulsating cavities, and to analyse the cavities stabilities just as the onset of cloud cavitation (Callenaere *et al.*, 1998).

A cartesian coordinate system (Oxy) is defined on the low channel bottom with the x-axis originating from the centre O of the elliptical nose and positive values indicating the direction downstream. The cavity length  $L$  is measured along the lower plate (T<sub>1</sub>Q) from the step origin T<sub>1</sub>.

The various measurement techniques are described in details in the very full article (Callenaere *et al.*, 2000). The characteristic velocity  $V_e$  in the lower channel is measured by Laser Doppler Velocimetry (LDV) in the middle of the section (Se) at  $x=0$ . Pressure fluctuations were measured with the use of 5 piezoelectric transducers located along the lower plate (T<sub>1</sub>Q) at the locations 50, 75, 100, 125 and 150 mm from the origin of the step. In order to measure the re-entrant jet thickness an ultrasonic technique was developed; most results were obtained with the 2.25 MHz ultrasonic transducer (PANAMETRICS ref. V306-SU and V311-SU).

In the inlet section (Si), situated at a distance of 280 mm from the leading edge I of the confinement plate, the total flow rate  $Q_t$  is obtained uniform and the velocity  $V_0$  unidirectional with the help of a converging section. For the computation of the cavitation number, the reference pressure  $P_r$  and velocity  $V_r$  are defined by the relations:

$$Q_t = (Se + Se') V_r \quad (1)$$

$$P_0 + 1/2 \rho V_0^2 = P_r + 1/2 \rho V_r^2 \quad (2)$$

$P_0$  is the pressure measured in the inlet section (Si) and  $\rho$  the water density. So the experimental cavitation number is defined as  $\sigma = (P_r - P_v) / (1/2 \rho V_r^2)$ , where  $P_v$  is the vapour pressure. Using (1) and (2) the pressure  $P_0$  is given by:

$$(P_0 - P_v) / (1/2 \rho V_r^2) = 1 + \sigma - [(Se + Se') / Si]^2 \quad (3)$$

We define the pressure coefficient with respect to the reference pressure and velocity as  $C_p = (P - P_r) / (1/2 \rho V_r^2)$ .

### 3. NUMERICAL MODELLING

The numerical results are obtained with the use of the Navier-Stokes codes FLUENT and STAR-CD. The two-dimensional calculation domain is limited by the (Si) inlet section and the (So) outlet section located at the abscissa of 1120 mm value. The domain mesh is constructed with the use of the FLUENT pre-processor.

The mesh of the domain, containing 15288 cells, has been realised by the connection of structured and unstructured different meshes. The figure 3 shows the entire mesh for a confinement height  $e = 20$  mm, a step height  $h = 10$  mm and a divergence angle  $\beta = 4.2^\circ$ .

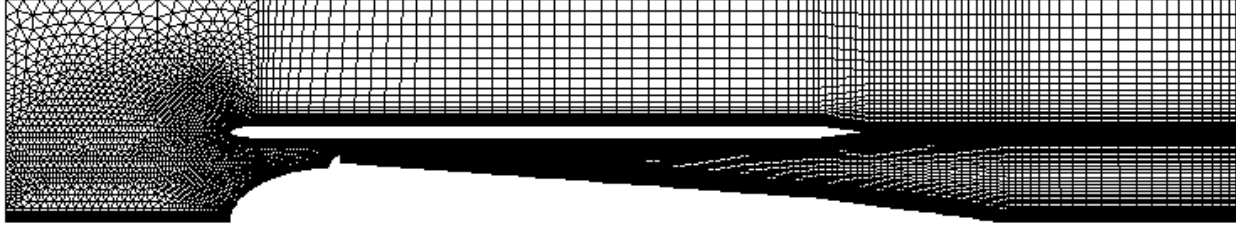


**Figure3. Mesh of the entire domain.**

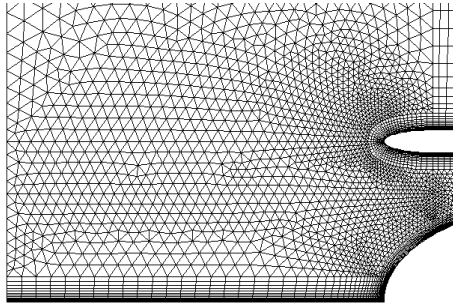


**Figure4. Upstream region.**

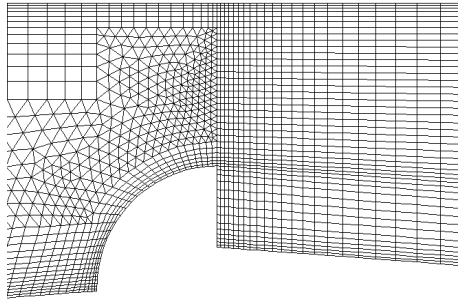


**Figure5. Cavity region.**

The mesh structure is triangular upstream the confinement plate (figure 4) and regular downstream the tiny obstacle, in the upper and lower channels (figures 3 & 5). The mesh is refined near the zones of strong gradients, in particular close to the cavity region (behind the step), close to the geometrical discontinuity zones and near the leading and trailing edges of the confinement plate. In order to intercept the walls boundary layers, a normal-wise progressive mesh has been used. The first cell height is 0.3 mm and the progression rate is equal to 1.2. The figure 5 illustrates the mesh refinement close to the step and the progression of the boundary layer mesh. A grid sensitivity study demonstrates that, a more refined grid does not influence significantly either the velocity field nor the pressure field.

One uses the well known semi-empirical  $k-\varepsilon$  model (Lauder & Spalding, 1972) to solve the transport equations for the turbulent kinetic energy  $k$  and its dissipation rate  $\varepsilon$ . In the case of the tunnel configuration, measurements show that the flow turbulence level is about 0.1 %. Because of the strong converging region, upstream, close to the inlet section (Si), the boundary layers are negligible, thus the inlet velocity is uniform. The boundary conditions are the followings: no-slip conditions on the walls, uniform pressure and velocity on the inlet section (Si), plus an outlet condition on the outlet section (So). The outlet condition consists of assuming a zero normal gradient for all flow variables except pressure.

The equations are integrated with respect to time using an implicit scheme. The velocity, pressure and void fraction are calculated at the cell centre. The SIMPLE algorithm is used for the pressure correction.

The flow calculation leads to a flow rate value different of those obtained experimentally. This gap is due to the head loss induced by the rods presence in the upper channel. In order to calculate the rods head loss, a porous medium is introduced in the upper channel, close to the cross-section (Sp) located at the middle of the confinement plate (figure 1). Thus, the region of interest (lower channel) is not disturbed. Across the (Sp) section, the flow velocity is unidirectional and uniform. So, the one-dimensional porous model, termed “porous jump”, is used to model a membrane coinciding with the section (Sp). The pressure jump,  $P_d - P_g$ , across the membrane is given as a combination of the Darcy’s law and an additional inertial loss term:

$$(P_d - P_g) / \rho v^2 = - A_1 - A_2 / v \quad (4)$$

Where  $v$  is the flow velocity normal to the membrane,  $A_1$  the pressure drop coefficient and  $A_2$  a term inversely proportional to the porous medium permeability. In the present study, the permeability value is assumed to be infinite, so the  $A_2$  coefficient disappears and the pressure jump becomes proportional to the dynamic pressure. The  $A_1$  coefficient can be viewed as a loss coefficient per unit length along the flow direction. For each calculation, the  $A_1$  value is calculated under non-cavitating configuration, then introduced as a known value in the calculation of the cavitating case. The  $A_1$  coefficient is adjusted such as the experimental value  $Q_e$  of the flow rate through the characteristic section (Se) is identical to those obtained by calculation.

Both for the VOF (STAR-CD) and the homogeneous (FLUENT) models, the mixture density is defined as  $\rho_M = \alpha \rho + (1-\alpha) \rho_v$ , where  $\rho_v$  is the vapour density and  $\alpha$  the volume fraction of the water. For the mixture the mass conservation equation gives the relation:

$$D\rho_M / Dt + \rho_M \nabla \cdot \mathbf{V} = 0 \quad (5)$$

$D/Dt$  is the material time derivative and  $\mathbf{V}$  the velocity vector at any point of the mixture. Assuming that the two phases are non-compressible, the equation (5), expressed in terms of the vapour volume fraction  $\alpha_v = 1 - \alpha$  becomes:

$$\rho_v [\partial \alpha_v / \partial t + \nabla \cdot (\alpha_v \mathbf{V})] = \rho_v D\alpha_v / Dt \quad (6)$$

The term,  $m'_v = \rho_v D\alpha_v / Dt$ , on the right-hand side, is the mass flow rate per unit volume between the water phase and the vapour phase. In order to close the models, one uses either the barotropic or the bubble cavitation model mentioned in paragraph 1.

#### *Barotropic model.*

Several assumptions are made: the liquid and vapour are in thermal equilibrium, the two phases are uniformly distributed within a cell, and that there is no sub-cell slip between the liquid and vapour. Using these assumptions, the energy equation is simplified to a barotropic equation:  $A_M^2 D\rho_M / Dt = DP / Dt$ . The two-phase speed of sound  $A_M$  is modeled using the classic homogeneous equilibrium model of Wallis (1969). Thus, the following equation of state is applied as a closure for the model (Schmidt *et al.*, 1997):

$$(P_v - P) / \rho a^2 = [(1 - 1/\xi) / (1 - \varpi^2)] \text{Log} [(\alpha + \varpi \xi \alpha_v) / (\alpha + \xi \alpha_v)] \quad (7)$$

Where,  $\xi = \rho_v / \rho$ ,  $\varpi = (\rho a / \rho_v a_v)^2$ ,  $a$  and  $a_v$  are the speed of sound in water and vapour respectively.

#### *Bubble model.*

This model allows the fluids to be interpenetrating and so mass to be transferred from one phase to another. It models the formation of bubbles when the local pressure becomes less than the vaporization pressure. Under isothermal conditions, the pressure within the bubble remains nearly constant and the change in bubble radius is approximated by a simplified Rayleigh equation (Kubota *et al.*, 1992):

$$dR / dt = \text{sign} (P_v - P) \cdot [2 |P_v - P| / 3 \rho ]^{1/2} \quad (8)$$

The total vapour mass per unit volume can be written:  $m_v = \rho_v \alpha_v = 4/3\pi R^3 N \rho_v$ , where  $N$  is the bubble number density per unit volume and  $R$  a typical bubble radius. Then, the term on the right-hand side of equation (6) is expressed as:  $m'_v / m_v = (3 / R) (dR / dt)$ , with  $1 / R = (4/3\pi N / \alpha_v)^{1/3}$ .

## 4. RESULTS

The experimental tests were carried out at the ambient temperature of 20°C. The water density  $\rho$  is equal to 998.21 kg/m<sup>3</sup>, the molecular viscosity  $\mu$  to 1.002 10<sup>-3</sup> kg/(m.s), the speed of sound  $a$  to 1531 m/s and the vapour pressure  $P_v$  to 2337 Pa. Under the saturated vapour condition, coming into the cavity, the vapour density  $\rho_v$  is equal to 1.73 10<sup>-2</sup> kg/m<sup>3</sup>, the molecular viscosity  $\mu_v$  to 0.88 10<sup>-5</sup> kg/m<sup>3</sup> and the speed of sound  $a_v$  to 378 m/s. All the herein results are obtained with the following parameters values. The divergence angle  $\beta$  is set equal to 4.2° and the  $Q_t$  total flow rate value to 170.72 l/s which leads to a 3.48 m/s value for  $V_0$ . The confinement plate is positioned at the fixed value  $e = 20$  mm which provides a 40.42 l/s value for the lower channel  $Q_e$  flow rate and the corresponding value of 11.55 m/s for the characteristic velocity  $V_e$ . For the given confinement height, the calculations are performed for the highest step height  $h = 10$  mm. When the bubble two-phase model is used the bubble number density per unit volume  $N$  is adjusted so that the calculation converges. The results are presented for a cavitation number  $\sigma$  equal to 3; the corresponding value of the  $P_r$  reference pressure is 46810 Pa.

In order to correctly initialise the calculation, a characteristic length value of the large turbulent structures is required. With regard to the present configurations, Schlichting (1970) estimates this length with the approximate law  $0.37 [v/V_0]^{0.2} \Delta^{0.8}$ , where  $\Delta = 30$  mm is the distance between the convergent outlet and the inlet section (Si). The characteristic length value is about 0.5 mm. In addition, the standard wall functions are based on the non-dimensional wall quantity  $y^+ = \rho V_t \delta / \mu$ , where  $V_t$  is the tangential velocity and  $\delta$  the normal-wise distance from the wall at any point of the domain. With the use of the boundary layer mesh, previously described (cf. §2), the  $y^+$  value of the wall-adjacent cells varies between 15 to 100, a range over which the classical log-law is valid.

Concerning the determination of the  $A_1$  coefficient of equation (4), the calculation shows that, without a porous medium ( $A_1 = 0$ ) the lower channel flow rate has a 26.01 l/s value, to be compared with the experimental one of 40.42 l/s. For the coefficient  $A_1 = 1$ , the calculated flow rate value is equal to the experimental one to within 1%.

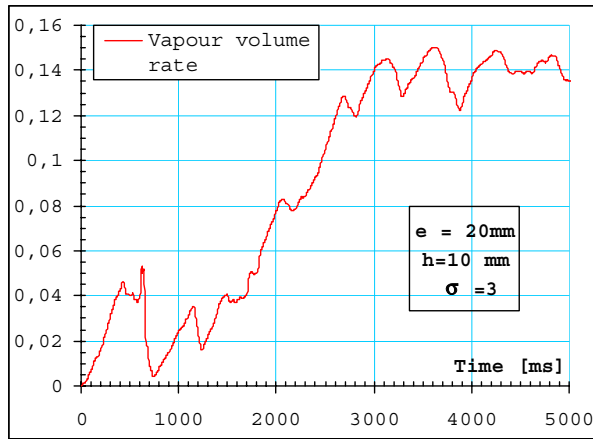


Figure 6. Time evolution of the vapour volume.

Both for the two codes, a non-cavitating calculation initialise the flow field. Under cavitating condition the time step is equal to 0.5 ms. A simulation of 5000 ms long is performed. The figure 6 presents the vapour volume rate evolution ( ratio of thecavity volume on the domain volume) versus time. During the first 800 ms the flow is strongly disturbed, due to the sudden start up of the cavity region. The vapour fills the detached flow region and then vanishes because of the non-steady behaviour of the flow. From  $t = 800$  ms to  $t = 3000$  ms the vapour volume rate increases; from this time to the end of the simulation it stabilises to a value of about 14%. Beyond  $t = 3000$  ms, the cavity volume oscillates continuously with an average period of 500 ms.

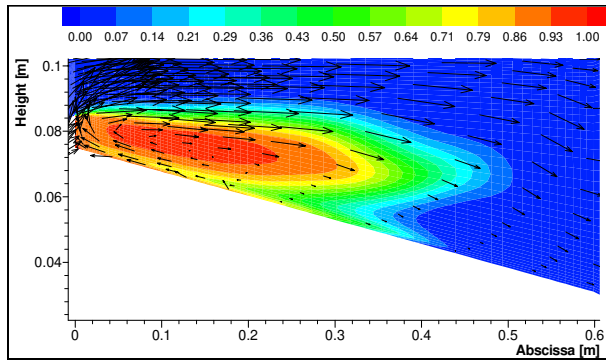


Figure 7. Cavity & velocity at time 1842 ms;  $\sigma = 3$ .

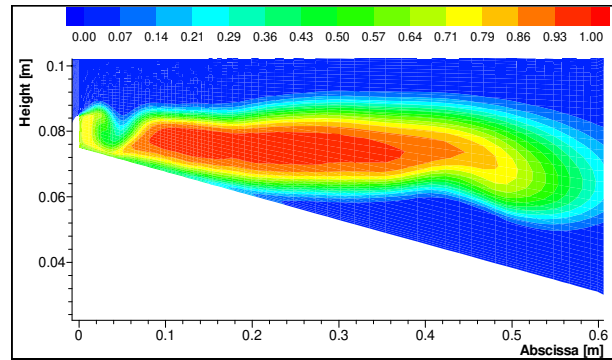


Figure 9. Cavity at time 2268 ms;  $\sigma = 3$ .

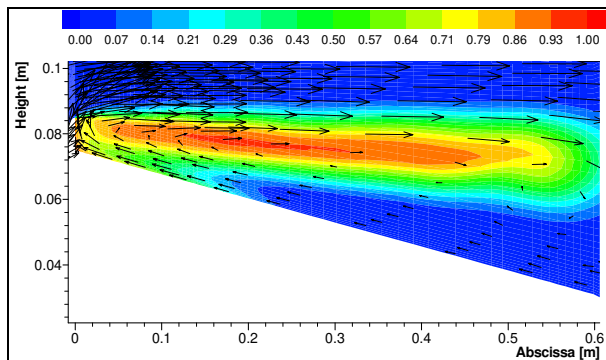


Figure 8. Cavity & velocity at time 1974 ms;  $\sigma = 3$ .

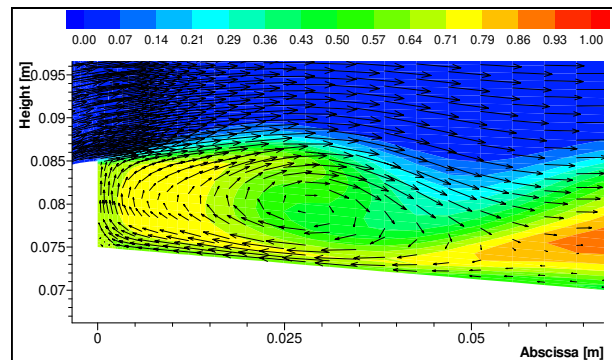


Figure 10. Cavity & velocity at time 2268 ms [zoom];  $\sigma = 3$ .

This instability corresponds to the vapour shedding in the flow. The figures 7 to 11 illustrate the cavity region and the flow field during one period of this phenomenon. At time  $t = 1842$  ms, the cavity grows; in the water and on the boundary cavity the  $x$  velocity is positive. At time  $t = 1974$  ms, the cavity is still increasing but a thick re-entrant jet appears with an important reverse flow. This is in agreement with the experimental observations (Franc, 2001). The time  $t = 2268$  ms corresponds to the very beginning of the shedding process. Two vapour vortices are present in the flow, the first in the new developing cavity just behind the step, and the second in a large cloud of bubbles detaching downstream (figure 10). This figure illustrates the counter-current flow with the velocity field distribution. The process goes on and at time  $t = 2292$  ms, the two vapour vortices are now clearly separated (figure 11).

The figure 12 shows x-velocities in the cross-section  $x = 300$  mm at the different times:  $t = 1788$ ,  $1842$  and  $1974$  ms. The re-entrant jet development is related to the change in velocity direction near the wall. At time  $t = 1974$  ms, the re-entrant jet thickness  $d_j$  is about  $15$  mm for a  $500$  mm value of the cavity length. The ratio  $d_j / L = 0.03$  is very close to the experimental one corresponding to a cavity length value of  $95$  mm.

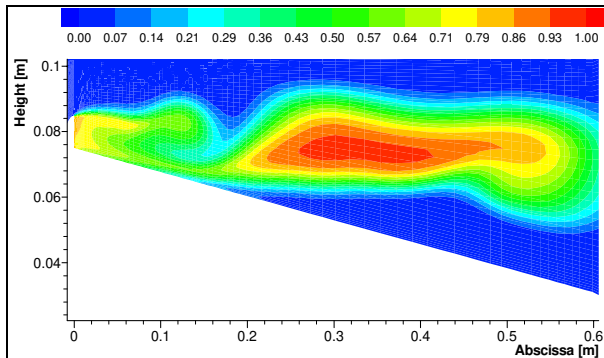


Figure 11. Cavity at time 2292 ms;  $\sigma = 3$ .

The experiments have highlighted that the re-entrant jet velocity can be considered as nearly constant all along its development. It covers a distance of about 75% of the maximum cavity length  $L_m$  during a time of about 40% of the shedding period  $T$ . Hence, its mean velocity is of the order of  $1.9 L_m/T$ . In the present case this relation yields a re-entrant jet velocity value of  $1.9$  m/s, to be compared with the  $1.6$  m/s value observed on the figure 12. The numerical Strouhal number  $L_m/[T.V_e]$  is found equal to  $0.1$ , the half of the usual experimental value.

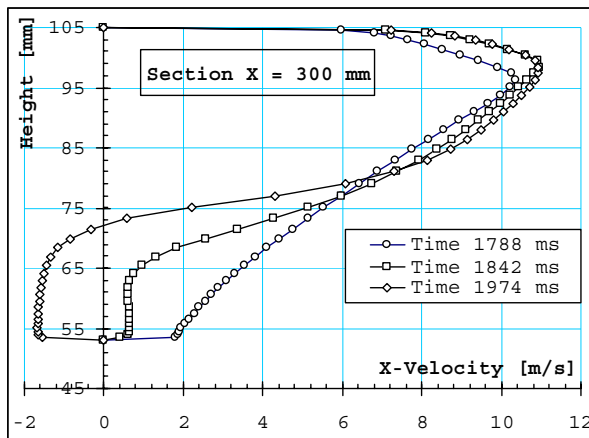


Figure 12. Velocity.  $e = 20$  mm;  $h = 10$  mm;  $\sigma = 3$ .

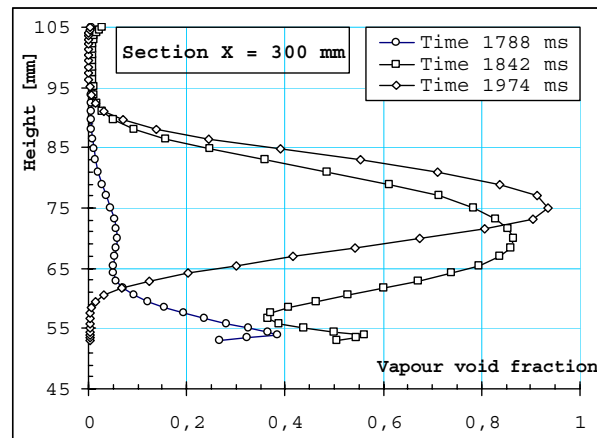


Figure 13. Void fraction.  $e = 20$  mm;  $h = 10$  mm;  $\sigma = 3$ .

The figure 13 illustrates the void fraction for the same cases considered in figure 12. Notice that the cavity is full of vapour only during the period where the re-entrant jet develops.

## 5. CONCLUSION

A complete simulation of a cavitating flow studied experimentally is performed. The use of the FLUENT solver has shown its ability to reproduce the typical dynamical behaviour of the cavity development, the re-entrant jet and the vapour shedding. The re-entrant jet velocity and thickness have been found close to the experimental values. The Strouhal number is the half of the value usually observed.

The numerical test case corresponds to a case of long cavity. The obtained results are very promising. The next calculations concern smaller cavities and other channel configurations. One of the goals is to reproduce by the calculation the experimental mapping of the cavitation regimes. It would be very interesting to obtain the different mapping regions: cloud cavitation with periodic instabilities, non auto-oscillating thin cavities with periodic re-entrant jet, cavitation surge, non auto-oscillating long cavities and shear cavitation.

## REFERENCES

- BRIANÇON-MARJOLLET L., MICHEL J.M., 1987.  
 "The hydrodynamic tunnel of I.M.G: former and recent equipments", FED, Vol 57, pp 37-47, Ed Holl J.W. & Billet M.L.  
 CALLENAERE M., FRANC J.P., MICHEL J.M., 1998.

"Influence of cavity thickness and pressure gradient on the unsteady behaviour of partial cavities", Proc. of the Third Int. Symp. on Cavitation, Vol 1., pp 209-214.  
 CALLENAERE M., FRANC J.P., MICHEL J.M., RIONDET M., 2000.  
 "The cavitation instability induced by the development of a re-entrant jet", J. Fluid Mech., Accepted, publication in progress, Sept 2000.  
 DIÉVAL L., ARNAUD M., MARCER R., 1998.  
 "Numerical modelling of unsteady cavitating flows by a VOF method", Proc. of the Third Int. Symp. on Cavitation, Vol 2, pp 243-248.  
 FRANC J.P., 2001.  
 "Partial cavity instabilities and re-entrant jet", Fourth Int. Symp. on Cavitation, Pasadena, USA, June 20-23, 2001.  
 FURNESS R.A., HUTTON S.P., 1975.  
 "Experimental and theoretical studies of two-dimensional fixed-type cavities", J. Fluids Eng., pp 515-522, December.  
 HIRT C.W., NICHOLS B.D., 1981.  
 "Volume of fluid (VOF). Method for the dynamics of free boundaries", J. Comput. Phys., Vol 39, pp 201-225.  
 KAWANAMI Y., KATO H., YAMAGUCHI H., TAGAYA Y., TANIMURA M., 1997.  
 "Mechanism and control of cloud cavitation", J. Fluids Eng., Vol 119, pp 788-795.  
 KNAPP R.T., DAILY J.W., HAMMITT F.G., 1970.  
 "Cavitation", Mc Graw-Hill, New-York.  
 KUBOTA A., KATO H., YAMAGUCHI H., 1992.  
 "A new modelling of cavitating flows: a numerical study of unsteady cavitation on a hydrofoil section", J. Fluid Mech., Vol 240, pp 59-96.  
 KUBOTA A., KATO H., YAMAGUCHI H., MAEDA M., 1989.  
 "Unsteady structure measurement of cloud cavitation on a foil section using conditional sampling technique", J. Fluids Eng. Vol 111, pp 204-210.  
 LAUNDER B.E., SPALDING D.B., 1972.  
 "Lectures in mathematical model of turbulence", Academic Press, London, England.  
 REBOUD J.L., DELANNOY Y., 1994.  
 "Two-phase flow modelling of unsteady cavitation", Proc. of the Second Int. Symp. on Cavitation, pp 39-44.  
 REBOUD J.L., STUTZ B., COUTIER O., 1998.  
 "Two-phase flow structure of cavitation: experiment and modelling of unsteady effects", Proc. of the Second Int. Symp. on Cavitation, Vol 1, pp 203-208.  
 SCHLICHTING H., 1970.  
 "Boundary layer theory", Mc Graw-Hill, New-York.  
 SCHMIDT D.P., RUTLAND C.J., CORRADINI M.M., 1997.  
 "A numerical study of cavitation flow through various nozzle shapes", Transactions of the SAE.  
 WALLIS G.B., 1969.  
 "One-dimensional two-phase flow", Mc Graw-Hill, p 143, New-York.  
 YAMAGUCHI H., KATO H., KAMIJO A., MAEDA M., 1990.  
 "Development of a laser holography system for the measurement of cavitation bubble clusters", ASME, Cavitation and Multiphase Flow Forum.